ARCHIVES OF ELECTRICAL ENGINEERING VOL. 74(1), pp. 165–189 (2025)

DOI 10.24425/aee.2025.153018

Stability and adaptability analysis of the traction power supply system with photovoltaic and energy storage under two access structures

CHUNYU WEI, XIN LI✉

School of New Energy and Power Engineering
Lanzhou Jiaotong University, Lanzhou 730070, China
e-mail: 12222139@stu.lzjtu.edu.cn, ✉ *lxfp167@163.com*

(Received: 15.06.2024, revised: 10.02.2025)

Abstract: The integration of photovoltaic and the energy storage system into traction power supply systems under railway power conditioner (RPC) or voltage source converter (VSC) access structures changes the original pure AC system into a hybrid AC/DC system. At the same time, which access structure of photovoltaic and the energy storage system has higher system stability and which has better adaptability are rarely mentioned in the stability analysis of traction power supply systems with photovoltaic and the energy storage system. Firstly, in this paper, impedance models for the two types of access structures of photovoltaic and energy storage systems are established, and the port impedance characteristics and stability influencing factors are analyzed from the aspects of system parameters and controller parameters. Second, combining the two typical working conditions of PV and the ESS access traction power system, from the perspective of stability, the robustness of the two access structures under the influence of negative impedance characteristics and the adaptability of access are compared. Compared to traditional stability analysis methods, the GMPM (Gain Margin and Phase Margin) criterion employed in this paper integrates both the dynamic characteristics and frequency response of the system, making it particularly suitable for small-signal stability analysis. Keeping the rest of the conditions the same under two typical working conditions, the RPC access structure has higher system stability when the two access structures input and output 35kW of active power, respectively. Finally, the simulation results in the MATLAB/Simulink simulation platform also confirm the better adaptability of the RPC access structure.

Key words: energy storage system, impedance model, photovoltaic, railway power conditioner, stability analysis, traction power supply system

1. Introduction

Table 1 explains some of the abbreviations used in the article.

Table 1. Abbreviations

Railway power conditioner	RPC
Voltage source converter	VSC
Photovoltaic	PV
Energy storage system	ESS

The traction power supply system represents a significant component of railway operation, with a notable impact on the overall energy consumption of railway transportation. It is projected that by 2030, the electrification rate of railways will exceed 78%. As the electrification rate of railways continues to rise, traction energy consumption is expected to experience a corresponding increase. In order to promote the low-carbon development of the railway industry, it is required that the total carbon emissions of railways peak in 2030. In addition, the scale of green railways, the proportion of green locomotives, and the proportion of green electricity use will gradually increase. Electrified railway development in high-altitude mountainous regions is currently experiencing significant expansion. This trend aligns with broader initiatives aimed at implementing low-carbon transportation infrastructure. As a result, there is an increasing focus on enhancing the quality of traction power supply in these challenging terrains. Additionally, the integration of renewable energy sources into newly constructed high-altitude mountain railway systems has emerged as a pressing consideration in the sector. Taking the Qinghai-Tibet Railway as an example, it passes through the solar energy resource-rich region in Northwest China, and there is a large amount of unused land along the railroad line that can be developed and utilized, so PV is very suitable to be accessed to the traction power supply system to alleviate the tense situation of energy supply and demand [1]. The integration of large-scale PV into traction power supply networks introduces new complexities. These systems must simultaneously manage the inherent fluctuations of traction loads and the variability of PV generation, both of which can impact the stability of the traction power supply system. In this context, the incorporation of the energy storage system (ESS) serves a dual purpose: mitigating the effects of these fluctuations and improving the utilization of regenerative braking energy. The situation is further complicated in regions characterized by weak local power grids, extended steep gradients, and other challenging topographical features, which can affect the stability of the traction network. Given these circumstances, the combined integration of PV and the ESS into the traction power supply system represents a significant area of focus in railway electrification strategies. For PV ESS access to the traction power supply system, Reference [2] proposes an active and reactive power combination trend control strategy, based on the ESS to maximize the regenerative braking energy and PV energy to make full use of. Reference [3] proposes a method for optimizing the capacity allocation of the PV ESS based on a technology-economic evaluation system, which can reduce the railway operating costs and improve the PV ESS utilization. In addition, after the access of the PV ESS, on the one hand, it can realize the large-scale utilization of renewable energy and nearby consumption, and on the other

hand, it can promote the transformation of the energy structure to the direction of multi-energy complementarity, laying a foundation for the construction of the Global Energy Internet [4].

The issue of traditional traction network power splitting can be addressed by integrating PV and the ESS into the traction power supply system through the RPC. This provides a conduit for the dynamic exchange of energy within the power supply area, thereby reducing reactive power and negative sequence hazards to a certain extent. In addition to the RPC access structure for PV and the ESS, it can also be connected to the traction power supply using the most mature VSC currently under research. PV and the ESS are connected to the traction power supply system via a DC bus. The AC bus on the locomotive side and the DC bus constitute an AC/DC hybrid system through the traction converter. As with microgrids based on PV and the ESS, the integration of PV and the ESS into traction power supply systems will inevitably result in a number of issues, including power quality problems, traction network voltage stability issues, traction network load prediction problems, and changes to the parameters of the original relay protection structure [5]. The existing research lacks an analysis of the impact of locomotive loads on the PV and ESS side after PV and the ESS is connected to the traction power supply system, as well as an analysis of the global impact of the intermittent PV on the original traction network and the impact on locomotive operating characteristics. Currently, the majority of related research is conducted by examining the coupling relationship and influencing the mechanism between the locomotive and the grid. For the RPC access structure, paper [6] first proposed to connect the photovoltaic array to the traction power supply through the RPC. Under the selection of an appropriate control strategy, this structure can compensate for the reactive power and negative sequence problems of the traction power supply system when connected to the traction power supply system, but it does not address the stability of the structure. In [7], a harmonic interaction analysis of the photovoltaic array connected to the traction power supply through the RPC was conducted, and a system harmonic current analysis model was established to investigate the harmonic interaction and adaptability of the PV-ESS- locomotive-grid coupling system. Nevertheless, the mechanism by which this structure affects stability was not investigated. The impedance model of the PV- locomotive-grid coupling system was established in [8] based on the above RPC access traction power supply system structure. Finally, a low-frequency stability analysis of the structure was carried out based on the extended forbidden zone criterion. Nevertheless, the structure did not consider system stability when the ESS was incorporated, and the impedance model on the AC side was unwieldy. References [9] and [10] present a systematic approach to establishing the AC side impedance model of the electrified railway locomotive-grid coupling system. The improved forbidden zone criterion and the improved sum-norm criterion are employed to analyze the stability of the established system. The conservativeness of the two criteria was analyzed, but the stability of the system was not analyzed with the PV and ESS structure connected. The study presented in [11] examines an integrated locomotive-grid coupling system utilizing a single-phase modular multilevel converter RPC. It introduces a novel third-order AC conductance model capable of capturing multi-harmonic characteristics. This model is applied to analyze the mechanisms behind low-frequency oscillations in the locomotive-grid coupling system. However, the research does not extend to an analysis of stability in the traditional RPC structure incorporating PV and ESS access. Additionally, it does not provide a comparative analysis of these traditional structures. Reference [12] proposes a coordinated control strategy for the RPC based on ESS integration, while robust stability analysis is performed for the system with conventional and coordinated control under forward and reverse

power flow, but in this paper, system stability analysis is performed only for the RPC structure with access to the ESS, and the integrated system stability under the influence of PV fluctuations is not taken into account. In [13], an ESS was integrated into the PV traction power supply structure based on RPC access. This not only optimized the consumption of the PV but also avoided the situation of power being sent back to the grid. Nevertheless, this paper did not examine the stability of the entire system following the addition of the ESS. For the VSC access structure, Reference [14] proposes a single-phase current control strategy based on the distributed photovoltaic power generation system connected to the AC bus through the VSC and then connected to the traction power supply system through the inverse V/V traction transformer, which can compensate for the three-phase unbalance. However, the literature does not analyze the stability of the three-phase photovoltaic power generation system connected to the traction power supply system. Reference [15] considered the asymmetric system of the three-phase structure of the traction power supply system accessing the grid, and deduced the locomotive single-input single-output impedance model applicable to the traction power supply system accessing the three-phase grid, but this paper only analyzes and studies the low-frequency oscillatory phenomenon of the locomotive-grid coupling, and does not consider the stability of the system under the access of PV and the ESS. The structure of the photovoltaic three-phase traction power supply system is the basis for the proposed hybrid traction power supply system scheme with integrated PV, as outlined in Reference [16]. In conjunction with the proposed power quality analysis method, the adaptability of the hybrid traction power supply system and the dynamic influence mechanism of each component are evaluated and analyzed, and the feasibility of the scheme is verified. The study examines the multi-factorial influence mechanisms affecting power quality in PV access traction power supply systems. However, the research does not extend to an analysis of the access scheme's adaptability from a system stability perspective. Reference [17] examined a three-phase access scheme and found that the scheme had no effect on three-phase unbalance, as verified by simulation. Nevertheless, the access capacity of PV will influence the three-phase voltage unbalance and output power factor. Additionally, this paper does not examine the access scheme from a stability standpoint. Reference [18] proposed a new three-phase access traction power supply system structure and a three-stage distributed voltage coordination control strategy. This strategy addresses the traction network voltage limit problem and improves the overall power supply level.

In summary, the current literature on the stability of PV and the ESS using the RPC and VSC in traction power systems is still limited. While some studies have investigated new access structures and converter control strategies, they mainly focus on optimizing the static characteristics of the system and the control performance. However, from the perspective of system stability, there is a relative lack of studies that comparatively analyze the stability and adaptability of different access structures under typical working conditions. As railways are an important pillar of national economic development, the promotion of new energy for large-scale access to the traction power supply system has become an important part of the national energy security strategy. Therefore, the study of the stable access structure of PV and the ESS in traction power supply can promote the development and promotion of new energy technology in the field of traction power supply, and help to realize the "double carbon target", which is of great significance in scientific research and practice. In light of the aforementioned considerations, this paper will establish the impedance models of PV, the ESS, RPC, and VSC based on the two PV and ESS access structures of the RPC and VSC, and analyze the impedance characteristics of the RPC and VSC ports. Considering

the various working conditions during the actual operation of locomotives, the two most typical working conditions of the traction power supply system with PV and the ESS are selected to analyze the influence of the system parameter changes on the system stability under the two access structures, and based on the analysis of the influence mechanism, the stability and adaptability of PV and the ESS under the two access structures are compared and analyzed.

2. Impedance modeling with the traction power supply system with PV and ESS

The topology of the traction power supply system with the PV and ESS studied in this paper is shown in Fig. 1, including photovoltaic, the energy storage system, railway power conditioner (RPC) and three-phase voltage source converter (VSC).

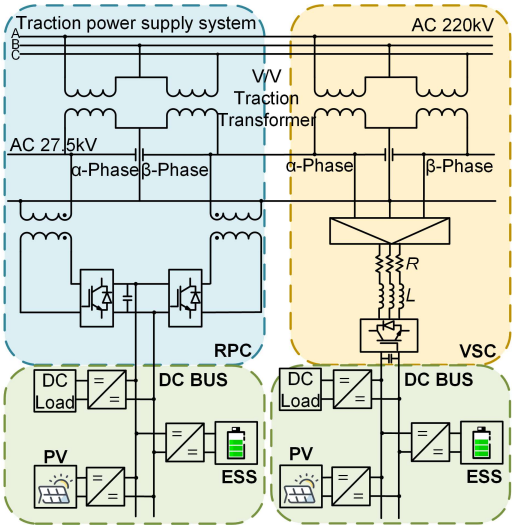

Fig. 1. The topology of the traction power supply system with PV and ESS (two access structures)

The traction power supply system under the RPC access structure is mainly composed of PV, the ESS, RPC, step-down transformer, etc. PV and the ESS are connected to the common capacitor in parallel through a DC/DC converter, and then connected to the DC side of the RPC through a DC bus, and the AC side is filtered and connected to a 27.5 kV traction feeder on both sides through a step-down transformer, etc. The traction power supply system under the VSC access structure mainly consists of PV, the ESS, VSC, PV-side transformer and so on. PV and the ESS are connected to the DC side of the VSC through the DC bus. The PV side transformer (2/3 transformer) adopts the inverse structure of the traction transformer (3/2 transformer) to provide three-phase symmetrical, sinusoidal, and stable grid-connected voltages to the VSC, and the AC side is filtered and spanned across the two sides of the 27.5 kV traction feeder.

2.1. Impedance modeling under RPC access structure

The system topology and control strategy in Fig. 2 show PV and the ESS connected to the traction power supply system based on the RPC.

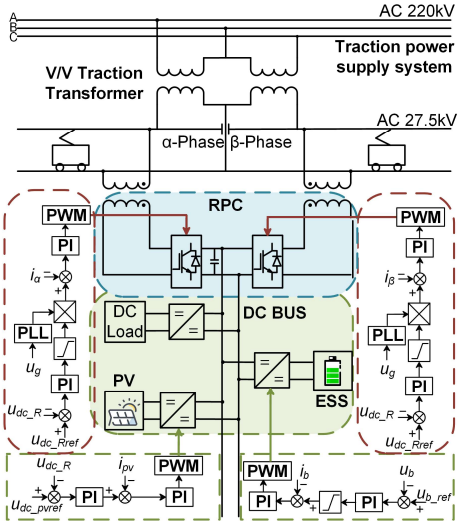

Fig. 2. The topology of the traction power supply system with PV and ESS under the RPC access structure

The impedance modeling of the DC–DC converter in this paper is based on the continuous conduction mode. On the PV output side, a boost circuit structure is used to connect to the DC bus. At the same time, PV is intermittent and uncertain, and the traction power supply system must ensure extremely high reliability and stability after commissioning. Therefore, in order to eliminate the uncertain effect of PV and ensure the safe operation of electrified railways, the PV unit must be equipped with an ESS connected to the DC bus through a bidirectional DC–DC circuit structure. According to the small signal modeling method, the secondary disturbance term is ignored and the small disturbance component is separated from the steady-state component to obtain the following small signal linear analytical model for PV and the ESS:

$$\begin{cases} L_{pv}\dfrac{\mathrm{d}\hat{i}_{pv}}{\mathrm{d}t} = \hat{u}_{pv} + (D_{pv}-1)\hat{u}_{dc\_pv} + U_{dc\_pv}\hat{d}_{pv} \\ C_{pv}\dfrac{\mathrm{d}\hat{u}_{dc\_pv}}{\mathrm{d}t} = (1-D_{pv})\hat{i}_{pv} - I_{pv}\hat{d}_{pv} + \hat{i}_{dc\_pv} \end{cases}, \tag{1}$$

$$\begin{cases} L_b\dfrac{\mathrm{d}\hat{i}_b}{\mathrm{d}t} + \hat{i}_b r_b = \hat{u}_b - U_{dc\_b}\hat{d}_b - D_b\hat{u}_{dc\_b} \\ C_b\dfrac{\mathrm{d}\hat{u}_{dc\_b}}{\mathrm{d}t} = I_b\hat{d}_b + D_b\hat{i}_b - \hat{i}_{dc_b} \end{cases}, \tag{2}$$

where L_{pv} is the inductance of the PV output side, i_{pv} is the PV output current, u_{pv} is the PV output voltage, C_{pv} is the energy storage capacitance on the PV DC bus side, u_{dc_pv} is the PV port DC output voltage, i_{dc_pv} is the PV port DC output current, and d_{pv} is the boost circuit duty cycle signal.L_b is the inductance of the ESS output side inductance, r_b is the ESS output side resistance, u_b is the ESS output voltage, i_b is the ESS output current, d_b is the bidirectional DC–DC circuit

duty cycle signal, C_b is the ESS DC bus side energy storage capacitance, u_{dc_b} is the ESS port DC output voltage, i_{dc_b} is the ESS port DC output current. Combining the control strategy in Fig. 2, the impedance model of PV and the ESS can be obtained:

$$Z_{pv\_\text{out}} = \frac{\hat{u}_{dc\_pv}}{\hat{i}_{dc\_pv}} = \frac{sL_{pv} + F_{pv}(s)}{A_{pv}s^2 + B_{pv}(s)s + \left(1 - D_{pv}\right)^2 + E_{pv}(s)}, \tag{3}$$

$$Z_{b\_\text{out}} = \frac{\hat{u}_{dc\_b}}{\hat{i}_{dc\_b}} = \frac{sL_b + F_{bat\_o}(s)}{A_{bat\_o}s^2 + B_{bat\_o}(s)s + E_{bat\_o}(s)}, \tag{4}$$

$$Z_{b\_\text{in}} = \frac{\hat{u}_{dc\_b}}{\hat{i}_{dc\_b}} = \frac{sL_b + F_{bat\_i}(s)}{A_{bat\_i}s^2 + B_{bat\_i}(s)s + E_{bat\_i}(s)}, \tag{5}$$

where:

$A_{pv} = C_{pv}L_{pv}$,
$B_{pv}(s) = U_{dc\_pv}G_{i\_pv}C_{pv} - I_{pv}G_{i\_pv}G_{v\_pv}L_{pv}$,
$E_{pv}(s) = (1 - D_{pv})^2 + (1 - D_{pv})(I_{pv}G_{i\_pv} + U_{dc\_pv}G_{i\_pv}G_{v\_pv})$,
$F_{pv}(s) = U_{dc\_pv}G_{i\_pv}$,
$A_{bat\_o} = C_bL_b$,
$B_{bat\_o}(s) = I_bG_{i\_bo}G_{v\_bo}L_b + C_br_b - U_{dc\_b}G_{i\_bo}C_b$,
$E_{bat\_o}(s) = I_bG_{i\_bo}G_{v\_bo}r_b + D_{bo}^2 - (U_{dc\_b}G_{i\_bo}G_{v\_bo} + I_bG_{i\_bo})D_{bo}$,
$F_{bat\_o}(s) = -U_{dc\_b}G_{i\_bo} + r_b$,
$A_{bat\_i} = C_bL_b$,
$B_{bat\_i}(s) = C_br_b + U_{dc\_b}G_{i\_bi}C_b$,
$E_{bat\_i}(s) = D_{bi}^2 - I_bG_{i\_bi}D_{bi}$,
$F_{bat\_i}(s) = -U_{dc\_b}G_{i\_bi} + r_b$.
$G_{i\_pv}(s) = k_{pi\_pv} + k_{ii\_pv}/s$ is the PV current loop transfer function.
$G_{v\_pv}(s) = k_{pv\_pv} + k_{iv\_pv}/s$ is the PV voltage loop transfer function.
$G_{i\_bo}(s) = k_{pi\_bo} + k_{ii\_bo}/s$ is the current loop transfer function in the ESS discharge state.
$G_{v\_bo}(s) = k_{pv\_bo} + k_{iv\_bo}/s$ is the voltage loop transfer function in the ESS discharge state.
$G_{i\_bi}(s) = k_{pi\_bi} + k_{ii\_bi}/s$ is the current loop transfer function in the ESS charging state and
$G_{v\_bi}(s) = k_{pv\_bi} + k_{iv\_bi}/s$ is the voltage loop transfer function in the ESS charging state.

Due to the symmetry of the RPC topology, only the α phase is selected for analysis. Taking the α phase as an example, a single phase can be equivalent to a single-phase full-bridge inverter. The small-signal linear analysis model of the α phase of the RPC is as follows:

$$\begin{cases} \hat{u}_g = 2U_{dc\_R}\hat{d}_R + (2D_R - 1)\hat{u}_{dc\_R} - L_R\dfrac{\mathrm{d}\hat{i}_{LR}}{\mathrm{d}t} \\ (2D_R - 1)\hat{i}_s + 2I_s\hat{d}_R = \hat{i}_{LR} \\ C_R\dfrac{\mathrm{d}\hat{u}_{dc\_R}}{\mathrm{d}t} + \hat{i}_s = \hat{i}_{dc\_R} \end{cases}, \tag{6}$$

where u_g is the grid voltage, u_{dc_R} is the RPC DC input voltage, i_{dc_R} is the RPC DC input current, L_R is the RPC filter inductance, C_R is the RPC DC energy storage capacitance, i_{LR} is the RPC AC output current, and d_R is the drive duty ratio of the two switches Q_1 and Q_4. In order to achieve stable energy transmission, it is important to ensure the stability of the DC bus voltage.

The outer loop control of the RPC access structure uses constant DC voltage control, and the inner loop current loop is the RPC output current control. According to the control strategy in Fig. 2, the RPC impedance model is:

$$Z_{R\_\text{in}} = \frac{\hat{u}_{dc\_R}}{\hat{i}_{dc\_R}} = \frac{(2D_R - 1)\,A_R(s)}{B_R(s) - E_R(s)A_R(s)}, \tag{7}$$

where

$A_R(s) = 2U_{dc\_R}G_{i\_R} + sL_R$,
$B_R(s) = (2D_R - 1 + 2U_{dc\_R}G_{v\_R}G_{i\_R})(2I_sG_{i\_R} + 1)$,
$E_R(s) = [2I_sG_{v\_R}G_{i\_R} - (2D_R - 1)C_Rs]$.
$G_{i\_R}(s) = k_{pi\_R} + k_{ii\_R}/s$ is the RPC current loop transfer function and
$G_{v\_R}(s) = k_{pv\_R} + k_{iv\_R}/s$ is the RPC voltage loop transfer function.

2.2. Impedance modeling under VSC access structure

Figure 3 shows the system topology and control strategy when PV and the ESS are connected to the traction power supply system based on the VSC.

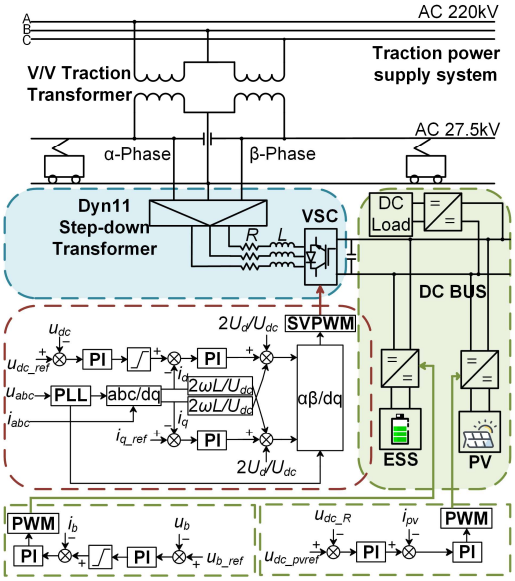

Fig. 3. The topology of the traction power supply system with PV and ESS under the VSC access structure

On the PV output side, a boost circuit structure is used to connect to the DC bus. The ESS is connected to the DC bus via a bi-directional DC–DC circuit structure. The DC bus is connected to the DC side of the VSC, and the rest is consistent with the RPC access topology. The modeling of PV and ESS impedance is the same as the RPC access structure. The small signal model of the VSC in the *dq* rotating coordinate system is as follows:

$$\frac{\mathrm{d}}{\mathrm{d}t}\begin{bmatrix}\hat{i}_d\\ \hat{i}_q\end{bmatrix} = \frac{1}{2L}\begin{bmatrix}D_d\\ D_q\end{bmatrix}\hat{u}_{dc\_\text{VSC}} + \frac{1}{2L_\text{VSC}}U_{dc\_\text{VSC}}\begin{bmatrix}\hat{d}_d\\ \hat{d}_q\end{bmatrix} - \begin{bmatrix}0 & -\omega\\ \omega & 0\end{bmatrix}\begin{bmatrix}\hat{i}_d\\ \hat{i}_q\end{bmatrix} - \frac{1}{L_\text{VSC}}\begin{bmatrix}\hat{u}_d\\ \hat{u}_q\end{bmatrix}, \tag{8}$$

$$\hat{i}_s = \frac{3}{4}\begin{bmatrix} D_d & D_q \end{bmatrix}\begin{bmatrix} \hat{i}_d \\ \hat{i}_q \end{bmatrix} + \frac{3}{4}\begin{bmatrix} \hat{d}_d & \hat{d}_q \end{bmatrix}\begin{bmatrix} I_d \\ I_q \end{bmatrix}, \tag{9}$$

$$C_{\text{VSC}}\frac{\mathrm{d}\hat{u}_{dc\_\text{VSC}}}{\mathrm{d}t} = \hat{i}_{dc\_\text{VSC}} - \hat{i}_s, \tag{10}$$

where: u_{dc_VSC} is the three-phase converter DC input voltage, R_{VSC}, L_{VSC} are the inverter output side resistance and filter inductance, id, iq are the inverter output current under the d and q axes, u_d, u_q are the inverter output voltage, d_d, d_q are the inverter duty cycle signals in the d and $q-$axes, and ω is the angular frequency. i_{dc_VSC} is the three-phase inverter DC input current, i_s the three-phase converter port input current, and C_{VSC} is the three-phase converter DC energy storage capacitance. Similarly, when PV and the ESS are connected to the traction power supply through the DC bus, a constant DC bus voltage control strategy is usually used to ensure the stability of the DC bus voltage. According to the control strategy in Fig. 3, the VSC impedance model is:

$$Z_{\text{VSC\_in}} = \frac{\hat{u}_{dc\_\text{VSC}}}{\hat{i}_{dc\_\text{VSC}}} = \frac{A_v(s)}{A_v(s)C_{\text{VSC}}s + B_v(s) + C_v(s) - D_v(s) + E_v(s)}, \tag{11}$$

where

$A_V(s) = 4U_{dc\_\text{VSC}}(U_{dc\_\text{VSC}}G_{i\_\text{VSC}}(s) + 2L_{\text{VSC}}s)$,
$B_V(s) = 3G_{v\_\text{VSC}}(s)G_{i\_\text{VSC}}(s)U_{dc\_\text{VSC}}(2I_dL_{\text{VSC}}s + D_dU_{dc\_\text{VSC}})$,
$C_V(s) = 6\omega L_{\text{VSC}}(I_qU_{dc\_\text{VSC}}G_{V\_\text{VSC}}(s)G_{i\_\text{VSC}}(s) + D_dI_q - D_qI_d)$,
$D_V(s) = 3U_{dc\_\text{VSC}}G_{i\_\text{VSC}}(s)(D_dI_d + D_qI_q)$,
$E_V(s) = 3U_{dc\_\text{VSC}}(D_d^2 + D_q^2)$,
$G_{i\_\text{VSC}}(s) = k_{pi\_\text{VSC}} + k_{ii\_\text{VSC}}/s$ is the VSC current loop transfer function, and
$G_{v\_\text{VSC}}(s) = k_{pv\_\text{VSC}} + k_{iv\_\text{VSC}}/s$ is the VSC voltage loop transfer function.

3. Impedance characteristics analysis of RPC and VSC ports

The traction converter in the traction power supply system with PV and the ESS can be equivalent to a flexible interconnection device. By connecting the DC bus with the AC bus through the flexible interconnection device, the bidirectional energy flow can be realized [19]. By classifying the locomotive operating conditions, two typical operating conditions are selected to analyze the impedance model and the overall system stability. Case 1 is the traction condition, in which energy flows from the DC side of the PV-ESS to the AC side of the locomotive through the traction converter and also flows to the DC load. Case 2 is the braking condition, in which energy flows from the AC side of the locomotive through the traction converter to the energy storage device and the DC load, and also from the PV side to the energy storage device and the DC load. This chapter analyzes the traction state.

3.1. Effect of system parameters on closed-loop input impedance

When the converter exchanges power with the outside world, the DC side capacitance of the converter can inhibit the fluctuation of the DC bus voltage to a certain extent by absorbing and releasing the energy [20]. Therefore, it is worthwhile to study in detail the influence mechanism

of the variation of the DC side capacitance parameters on the input impedance of the converter. The closed-loop input impedance of the RPC is selected for study and analysis, keeping other parameters unchanged, when the value of the DC side capacitance is varied from 5 mF to 100 mF, the input impedance bode plot of the RPC is shown in Fig. 4(a).

As shown in Fig. 4(a), in the medium and high frequency bands, the phase angle of the RPC's closed-loop input impedance does not change with the change of the DC side capacitance, and a negative impedance characteristic appears. In the low-frequency band, as the DC side capacitance value increases, the resonance peak of the RPC's closed-loop input impedance does not change, and the resonance frequency gradually decreases. As the DC side capacitance value increases, the phase of the RPC's closed-loop input impedance changes faster with frequency, but this does not affect the stability of the RPC's closed-loop input impedance.

The VSC closed-loop input impedance is selected for analysis and other parameters are held constant. Figure 4(b) shows the bode plot of the VSC closed-loop input impedance as the value of the DC-side capacitance varies from 2 mF to 100 mF.

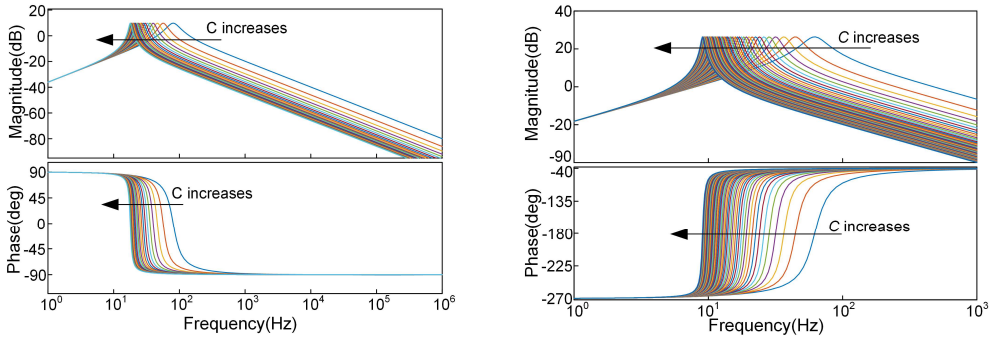

(a) RPC (b) VSC

Fig. 4. Bode plot of RPC and VSC closed-loop input impedance with varying capacitance on the DC side

It can be seen that in the mid-frequency and high-frequency bands, the phase angle of the closed-loop input impedance of the VSC does not change with the change of the DC side capacitance, and exhibits a negative impedance characteristic in the full-frequency band. In the low-frequency band, the resonance peak of the closed-loop input impedance of the VSC does not change as the DC side capacitance value increases, while the resonance frequency gradually decreases. As the DC side capacitance value increases, the phase of the VSC's closed-loop input impedance changes faster with frequency, but it does not affect the stability of the VSC's closed-loop input impedance.

3.2. Effect of voltage-current loop factor on closed-loop input impedance

When PV and the ESS access the traction power system through the RPC, it is necessary to control the two single-phase inverters. This is because changes in the current and voltage loop factors will affect the system's stability. To investigate this, the RPC closed-loop input impedance

was selected for analysis. The other parameters were kept constant. When the value of the voltage loop scaling factor K_p increased from 0.01 to 0.5, the bode plot of the RPC closed-loop input impedance is shown in Fig. 5(a).

As can be seen from Fig. 5(a), in the low-frequency band, the resonance peak of the RPC closed-loop input impedance decreases gradually as the voltage loop scaling factor increases, and at the same time, the phase angle of the RPC closed-loop input impedance tends to flatten out gradually with the change of frequency. Figure 5(b) shows the bode plot of the RPC closed-loop input impedance when keeping other parameters unchanged, and when the value of the voltage loop integration factor K_i increases from 2 to 100.

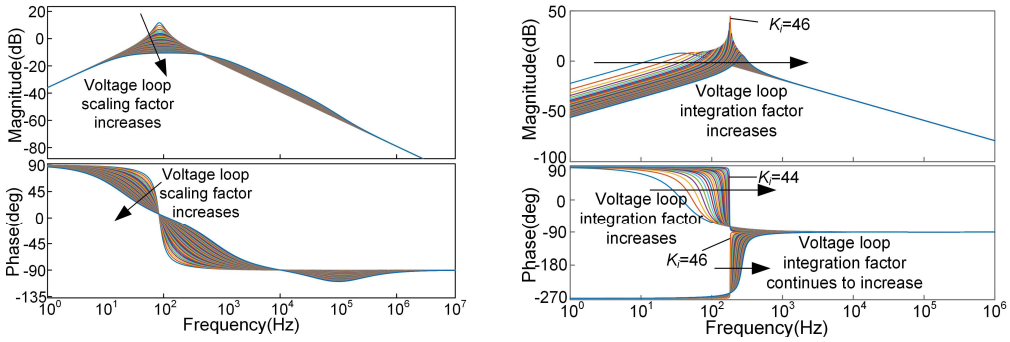

(a) Voltage loop scaling factor (b) Voltage loop integration factor

Fig. 5. Bode plot of RPC closed-loop input impedance as the voltage loop scaling factor and integration factor varies

In the low-frequency band, the resonance peak of the RPC closed-loop input impedance gradually increases with an increase in the voltage loop integration factor and reaches the maximum when the value of the voltage loop integration factor, K_i, is increased to 46. The resonance peak gradually decreases as the integration factor continues to increase, while the phase angle of the RPC closed-loop input impedance gradually tends to be non-flat with frequency. After the integration factor is increased to 46, the RPC closed-loop input impedance exhibits negative impedance characteristics in the full frequency band. It is verified that the magnitude and phase of the RPC closed-loop input impedance basically do not change with the change of current loop scaling factor and current loop integration factor.

When PV and the ESS are connected to the traction power supply through the form of the VSC, the closed-loop input impedance of VSC is selected for the study and analysis. Figure 6(a) shows the bode plot of the closed-loop input impedance of the VSC when keeping the other parameters unchanged, and when the value of voltage loop scaling factor K_p increases from 0.2 to 5.

From Fig. 6(a), it can be seen that in the low-frequency band, the resonance peak of the VSC closed-loop input impedance gradually decreases with an increase in the voltage loop scaling factor, while the phase angle of the VSC closed-loop input impedance tends to gradually flatten with the change of frequency. Figure 6(b) shows the bode plot of the VSC closed-loop input impedance as the value of the voltage loop integration factor K_i increases from 2 to 100.

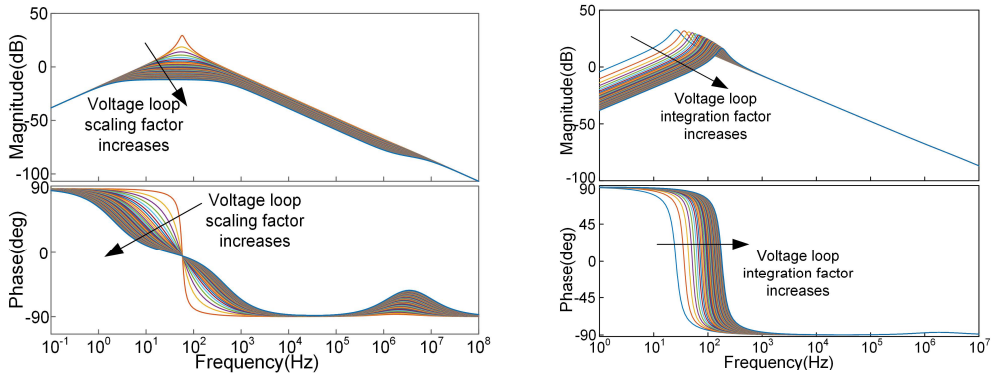

(a) Voltage loop scaling factor (b) Voltage loop integration factor

Fig. 6. Bode plot of VSC closed-loop input impedance as the voltage loop scaling factor and integration factor varies

In the low-frequency band, as the voltage loop integration factor increases, the resonance peak of the VSC closed-loop input impedance gradually decreases and the resonance frequency gradually increases. At the same time, the phase angle of the VSC closed-loop input impedance gradually becomes steeper as the frequency changes. It has been verified that the magnitude and phase of the VSC closed-loop input impedance basically do not change with the change of current loop scaling factor and current loop integration factor.

4. Stability analysis of traction power supply system with PV and ESS under typical operating conditions

This chapter combines the traction and braking conditions of the actual operation of the locomotive, and under these two typical conditions, based on the RPC and VSC two-way PV-ESS access traction power supply system structure, the stability of the AC/DC hybrid system is analyzed.

4.1. Stability analysis method

In analyzing the stability of small signals in the system, the Middlebrook criterion was first used to determine the stability of the system impedance ratio. However, because it requires the system to satisfy the condition that the equivalent output impedance of the source subsystem is much smaller than the equivalent input impedance of the load subsystem throughout the frequency band [21], it is too conservative in actual application, and the actual system cannot satisfy the conditions of the criterion. Therefore, the GMPM (gain margin and phase margin) criterion, which is an improved version of the Middlebrook criterion, states that when the polar plot of the system impedance ratio $Z_o(s)/Z_i(s)$ is outside the forbidden region, the stability of the system can be guaranteed, and the system can ensure 6 dB magnitude margin and 60° phase margin [22]. The GMPM criterion narrows the range of the impedance ratio prohibited region and reduces the design conservatism. For the topology and model of the traction power supply system with PV and the ESS,

the magnitude and phase angle of the equivalent input impedance of the power-side subsystem of the system, the equivalent input impedance of the load-side subsystem can be acquired. Therefore, it is important to use this criterion to analyze the stability of the system, and lays the theoretical foundation for the stability analysis of the traction power supply system with PV and the ESS. The sub-loop gain of the traction power supply system with PV and the ESS in this paper is:

$$T(s) = \frac{Z_o(s)}{Z_i(s)}, \tag{12}$$

where $Z_o(s)$ is the output impedance of the source subsystem under different operating conditions and $Z_i(s)$ is the input impedance of the load subsystem under different operating conditions. Therefore, it is only necessary to ensure that the Nyquist curve of $T(s)$ does not enter the forbidden region to ensure the stability of the system. The system parameters are listed in Table 2.

Table 2. System parameters for traction power supply system with PV and ESS

Module	**Parameter symbol**	**Parameter value**	**Module**	**Parameter symbol**	**Parameter value**
Line parameters	R_{line}/Ω, X_{line}/Ω	0.1, 0.2	RPC	C_R/μF	5000
Boost converter	C_{pv}/μF	200		L_R/H	0.01
	L_{pv}/H	0.0025		k_{pv_R}, k_{iv_R}	0.02, 10
	k_{pv_pv}, k_{iv_pv}	0.02, 0.2		k_{pi_R}, k_{ii_R}	1, 6
	k_{pi_pv}, k_{ii_pv}	0.15, 146	VSC	C_{VSC}/μF	2200
Bidirectional DC–DC	C_{ess}/μF	200		L_{VSC}/H, C_{VSC}/μF	0.005, 220
	L_{ess}/H	0.1		k_{pv_VSC}, k_{iv_VSC}	0.2, 10
	k_{pv_ess}, k_{iv_ess}	0.02, 1.3		k_{pi_VSC}, k_{ii_VSC}	25, 888
	k_{pi_ess}, k_{ii_ess}	0.5, 50			

4.2. Equivalent circuits for two typical operating conditions

The impedance stability analysis of the traction power supply system with PV and the ESS requires the derivation of the equivalent impedance circuits according to two typical operating conditions, and the stability analysis of different access structures is performed under the assumption that there is sufficient light for each access structure. The mains voltage is converted to the AC bus

side and the locomotive is equivalent to a constant power load. Taking the RPC and VSC two-way PV and ESS access traction power supply system structure as an example, based on the traction conditions of the locomotive, if the output of the PV-ESS is used as the "source" and the input of the converter is used as the "load", when the traction power required by the locomotive is large, the energy gap that cannot be provided by PV and the ESS will be supported by the grid. The equivalent circuits under traction conditions are shown in Figs. 7 and 8.

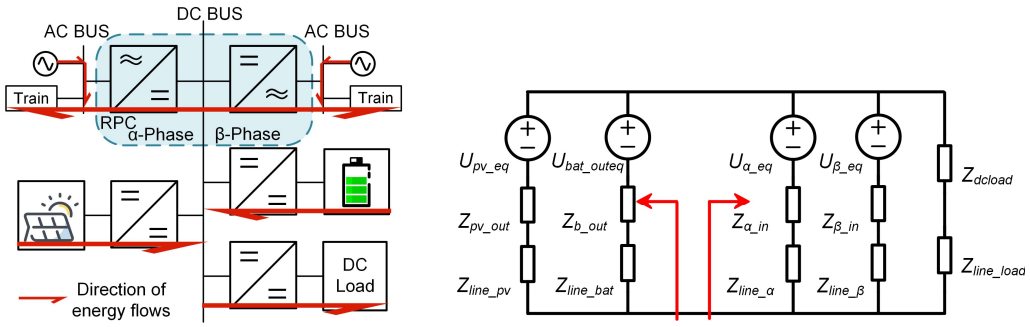

(a) Schematic diagram of energy flow (b) Thevenin equivalent circuit

Fig. 7. The traction power supply system with PV and ESS under the RPC access structure

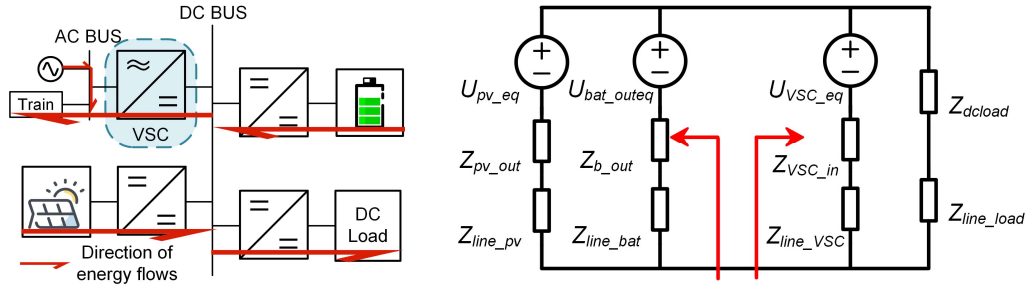

(a) Schematic diagram of energy flow (b) Thevenin equivalent circuit

Fig. 8. The traction power supply system with PV and ESS under the VSC access structure

When the locomotive is in braking condition, the Thevenin equivalent circuit is similar to the above. Set the line impedance to: $Z_{\text{line}} = R_{\text{line}} + jX_{\text{line}}$, so that:

$$
\begin{aligned}
Z_{pv\_eq} &= Z_{pv\_\text{out}} + Z_{\text{line}\_pv},\\
Z_{bat\_\text{in}eq} &= Z_{b\_\text{in}} + Z_{\text{line}\_bat},\\
Z_{bat\_\text{out}eq} &= Z_{b\_\text{out}} + Z_{\text{line}\_bat},\\
Z_{dc\_eq} &= Z_{dc\text{load}} + Z_{\text{line}\_\text{load}},\\
Z_{\alpha\_eq} &= Z_{\alpha\_\text{in}} + Z_{\text{line}\_\alpha},\\
Z_{\beta\_eq} &= Z_{\beta\_\text{in}} + Z_{\text{line}\_\beta},\\
Z_{\text{VSC}\_eq} &= Z_{\text{VSC}\_\text{in}} + Z_{\text{line}\_\text{VSC}}.
\end{aligned}
$$

Therefore, the equivalent impedance under typical operating conditions for the two access structures is shown in Table 3.

Table 3. Equivalent impedance of PV-ESS access based on RPC and VSC structure

	RPC traction condition	**RPC braking condition**	**VSC traction condition**	**VSC braking condition**
Equivalent output impedance	$Z_{\text{RPC\_out}} = Z_{pv\_eq} \| \| Z_{bat\_outeq}$	$Z_{\text{RPC\_out}R} = -Z_{pv\_eq} \| \| Z_{\alpha\_eq} \| \| Z_{\beta\_eq}$	$Z_{\text{VSC\_out}} = Z_{pv\_eq} \| \| Z_{bat\_outeq}$	$Z_{\text{VSC\_out}R} = -Z_{pv\_eq} \| \| Z_{\text{VSC\_}eq}$
Equivalent input impedance	$Z_{\text{RPC\_in}} = Z_{\alpha\_eq} \| \| Z_{\beta\_eq} \| \| Z_{dc\_eq}$	$Z_{\text{RPC\_in}R} = Z_{bat\_ineq} \| \| Z_{dc\_eq}$	$Z_{\text{VSC\_in}} = Z_{\text{VSC\_}eq} \| \| Z_{dc\_eq}$	$Z_{\text{VSC\_in}R} = Z_{bat\_ineq} \| \| Z_{dc\_eq}$

4.3. Analysis of factors affecting stability under changing system parameters

According to the data in Table 1, the DC bus voltage level is set to 700 V. Since the DC side capacitance plays an important role in establishing the energy transmission link between the DC and AC sides, then, when the locomotive is in traction conditions, the DC side capacitance is changed to observe the stability change trend under the two access structures of the RPC and VSC, as shown in Fig. 9.

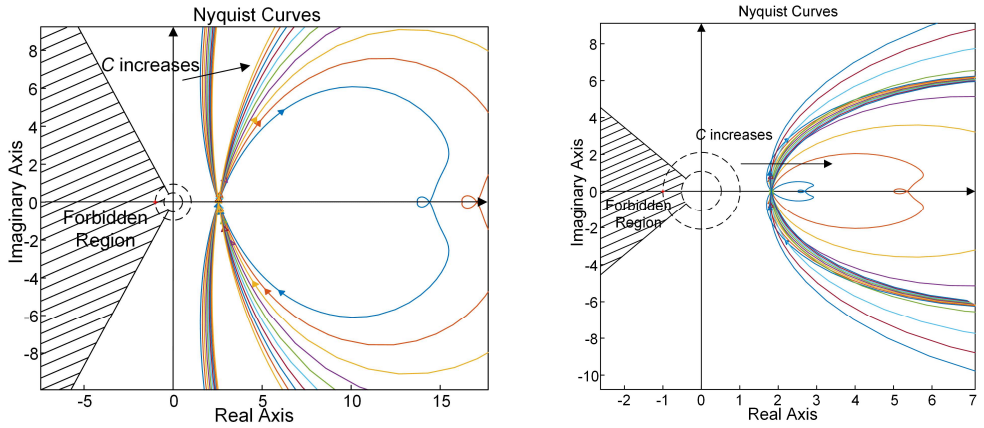

(a) RPC (b) VSC

Fig. 9. Variation trend of the Nyquist curve of the impedance ratio of the RPC and VSC access structure under traction condition with the change of the DC side capacitance

Analyzing the above figure, as the DC side capacitance gradually increases, the impedance ratio of the two access structures gradually moves away from the forbidden region on the Nyquist curve. Therefore, increasing the DC side capacitance under the two access structures accordingly can improve the system stability. The Nyquist curves for the RPC and VSC access structures when the locomotive is in braking condition are shown in Fig. 10.

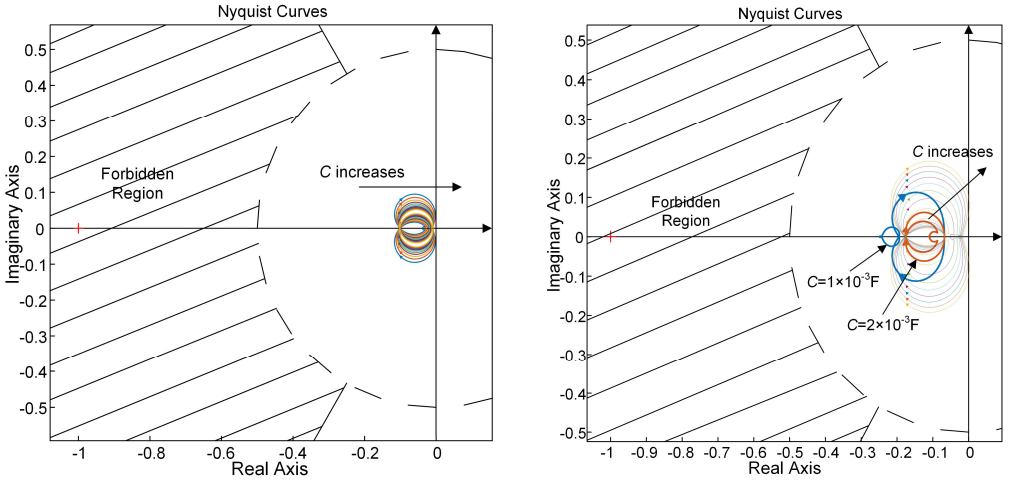

(a) RPC (b) VSC

Fig. 10. Variation trend of the Nyquist curve of the impedance ratio of the RPC and VSC access structure under braking condition with the change of the DC side capacitance

As can be seen from the figure, under braking condition, the impedance ratio of the RPC access structure moves away from the forbidden region with an increase in the DC side capacitance, and the system stability of the RPC access structure can be improved by appropriately increasing the DC side capacitance. Observing the VSC access structure, when the DC side capacitance is increased from 1×10^{-3} F to 2×10^{-3} F, the impedance ratio of the VSC access structure is far from the forbidden region on the Nyquist curve, but when the DC side capacitance is further increased, the curve approaches the forbidden region.

The above analysis is basically the same as the situation reflected by the actual system. The DC side capacitance is important for establishing a stable DC bus voltage and is also the basis for the converter to ensure stable transmission of DC side power. Therefore, selecting an appropriate DC side capacitance can effectively improve the stability of the traction power system with the addition of PV.

5. Analysis of the adaptability of two PV-ESS access structures from the perspective of system stability

As a new structure in the field of traction power supply research, the RPC has great potential due to its modular expandability, easy controllability, and superior negative sequence reactive power compensation capabilities. The VSC is a traditional grid-connected PV structure, and research on its control strategy, operation characteristics, and fault analysis has been relatively in-depth. However, due to the structure of the VSC itself, when the traction network is unloaded or lightly loaded, the current backflow phenomenon will occur. At the same time, under the influence of the double uncertainties of PV and traction loads, power quality problems such as

three-phase unbalance will be aggravated [5]. When PV and the ESS are connected to the traction power supply system with a VSC, the absorption rate of PV power will be reduced because the PV power of the two arms cannot be dynamically adjusted, and the occurrence of the light abandonment phenomenon will indirectly reduce the economic benefits [23].On the contrary, the special structure of the two arms of the RPC combined with the charging and discharging capacity of the ESS can effectively suppress the negative sequence current and two-arm harmonics in the traction power supply system [24], thereby improving the output power factor reduced by the PV access, and ensuring the economic benefits of the PV-ESS access to the traction power supply system from the perspective of reducing the occurrence of light rejection. However, due to the access of the ESS to the traction power supply system, the repeated charging and discharging of the ESS will generate new power flows, which will lead to an increase in the complexity of the RPC and control strategies [25]. In summary, it is not sufficient to draw conclusions from the advantages and disadvantages of the two access structures alone, so it is necessary to conduct in-depth research in combination with system stability analysis.

5.1. Comparison of the stability of the two access structures under typical operating conditions

To analyze the system stability of the two access structures under two typical operating conditions, the sum of the active power output of the two arms of the RPC and the active power output of the VSC is set to 35 kW, and the active power output of the two arms of the RPC is equal. When the same capacity of PV and the ESS are connected to the traction power supply system through the same voltage level DC bus, the impedance ratio Nyquist curves of the two access structures under traction and braking conditions are drawn on the same plane, as shown in Fig. 11(a).

As shown in Fig. 11(a), when the output is equal to the active power, the Nyquist curve of the impedance ratio of the RPC structure is farther away from the forbidden region than the VSC structure. Therefore, when the locomotive is in traction conditions, the RPC access structure has higher system stability. When the locomotive is in braking conditions, the sum of the active power input of the two arms of the RPC and the active power input of the VSC are both 35 kW, as shown in Fig. 11(b).

When the same input active power is set, the Nyquist curves of the impedance ratio of the RPC and VSC access structures are closer to the forbidden region than the Nyquist curves in the traction condition. However, in the braking condition, the Nyquist curves of the impedance ratio of the VSC access structure are closer to the forbidden region, so when the locomotive is in the braking condition, the RPC access structure also has higher system stability.

Constant power loads (CPLs) have negative damping characteristics. When CPLs are connected to the DC bus, they affect the stability of the system, reducing the system stability margin and system damping [26]. Therefore, CPLs can be connected to the DC bus side under the two access structures, and the robustness of the two access structures can be verified by increasing the access capacity of the CPLs. The DC bus's ability to withstand pressure can be measured and the access structure with a higher system stability margin can be determined. When the capacity of the CPL is gradually increased to the same extent in the two access structures, the trend of stability changes is observed.

In Fig. 12(a), under the RPC access structure, the RPC impedance ratio Nyquist curve first gradually shifts to the forbidden zone as the CPL access capacity increases. This indicates that the risk of system instability gradually increases with an increase in the CPL capacity while the

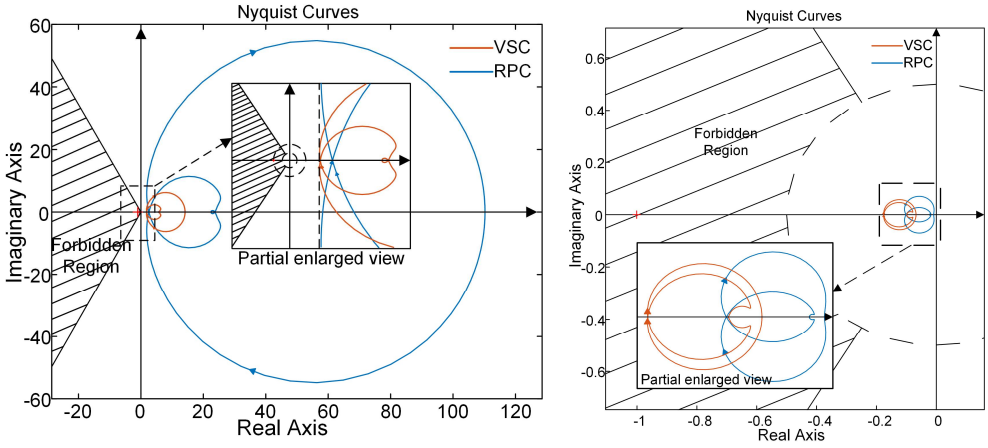

(a) Traction condition (b) Braking condition

Fig. 11. Nyquist curve of impedance ratio of RPC and VSC access structures under traction condition and braking condition

stability margin gradually decreases. As the access capacity continues to increase, the Nyquist curve enters the forbidden region, and the system is unstable. In Fig. 12(b), the system is in a stable state except when the CPL is not connected.

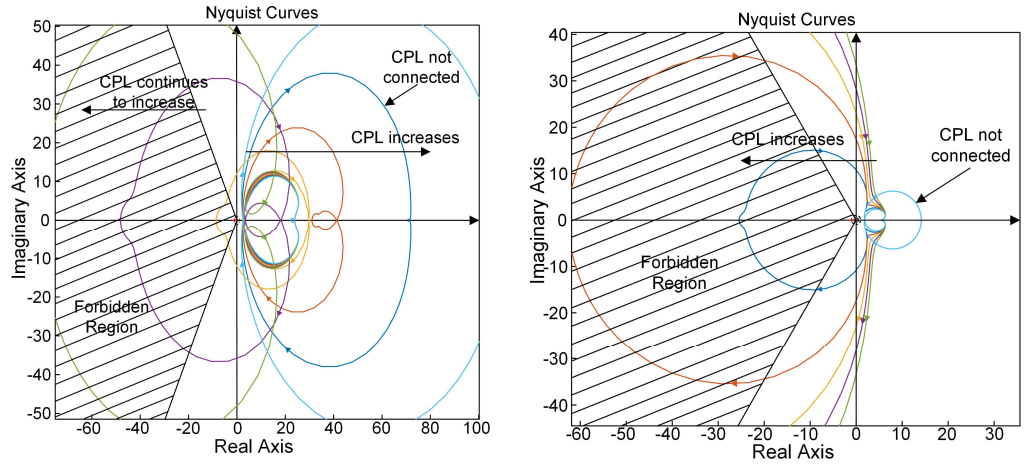

(a) RPC (b) VSC

Fig. 12. Nyquist curve of impedance ratio of RPC and VSC access structure when the CPL access capacity increases under traction condition

As the CPL access capacity increases, the Nyquist curve of the impedance ratio of the VSC gradually moves away from the right half plane, and the system is unstable.

Similarly, as shown in Fig. 13, under the RPC access structure, as the CPL access capacity increases, the RPC impedance ratio Nyquist curves in the complex plane gradually move to the left-hand side of the forbidden region, and the risk of system destabilization gradually increases.

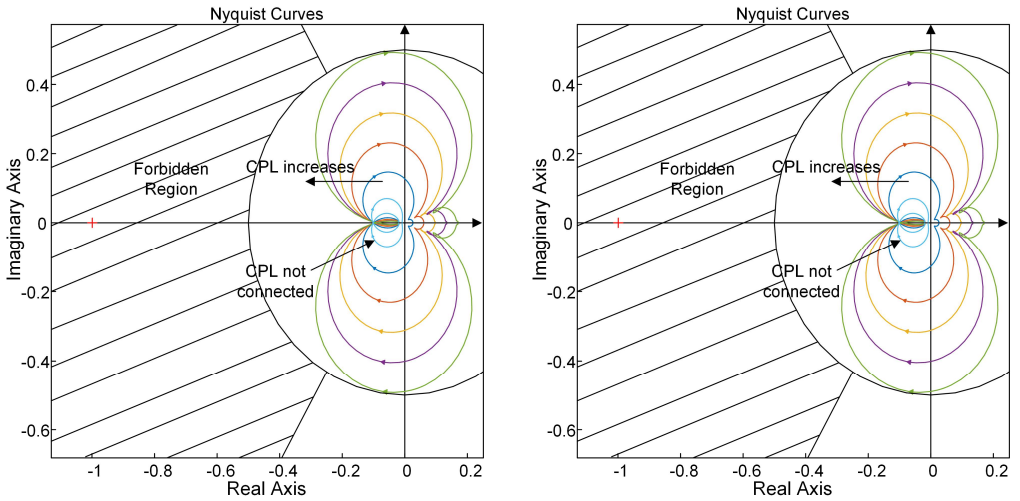

(a) RPC (b) VSC

Fig. 13. Nyquist curve of impedance ratio of RPC and VSC access structure when the CPL access capacity increases under braking condition

None of the curves crosses into the forbidden region, so the system remains stable for all CPL access capacities analyzed. Under the VSC access structure, as the CPL access capacity increases, the Nyquist curve of the VSC impedance ratio has a tendency to shift to the left in the complex plane, the risk of system instability gradually increases, and the system stability margin decreases. As the access capacity increases further, the Nyquist curve enters the forbidden region and the system is destabilized.

The RPC has the characteristic of realizing the transmission of energy to the two power supply arms. Unlike the VSC, the RPC access structure can output unequal active power by controlling the two converters separately. After the PV power is connected to the RPC through the DC bus, the problem of active power feedback in the traction power supply system can be solved by outputting unequal active power to the two arms, and the maximum utilization of the PV can also be realized [20]. Therefore, the imbalance between the output and input of the two arms of the RPC under two typical operating conditions also needs to be studied, and the stability change trend is observed when the output and input power of the two arms are unbalanced under the RPC access structure.

As shown in Fig. 14, when the transmission power of the two arms of the RPC is unbalanced and the degree of unbalance gradually increases, the Nyquist curve of the impedance ratio of the RPC access structure under the two typical operating conditions does not change with an increase in the transmission power unbalance degree, so when the output of the two arms is unbalanced under the RPC access structure, the system stability basically does not change.

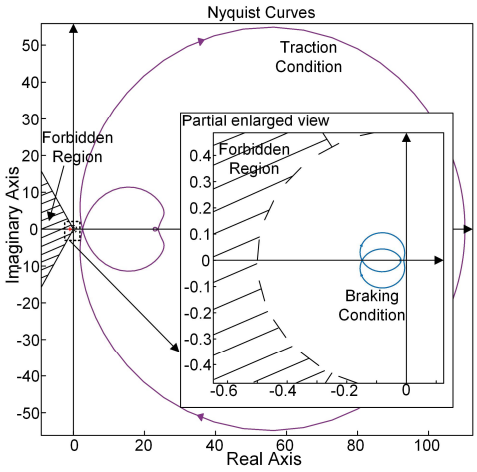

Fig. 14. Impedance ratio Nyquist curve when the output of the two arms of the RPC is unbalanced under traction and braking conditions

5.2. Adaptability analysis of two access structures

By analyzing the Nyquist curves of the impedance ratios of the two PV-ESS access structures, the RPC and VSC, under the two conditions of traction and braking, when the input and output power of the two structures are the same and the capacity of the connected PV and ESS is the same, the RPC access structure is farther away from the forbidden region than the VSC access structure, so it can be judged from the perspective of system stability that the RPC access structure has higher stability than the VSC access structure. At the same time, under the traction and braking conditions, the same capacity of the CPL with negative damping characteristics is connected to the DC bus side. As the capacity of the CPL increases by the same amount, the VSC access structure loses stability before the RPC access structure, so the RPC access structure has better system robustness than the VSC access structure. When the power transmitted by the two arms of the RPC is unbalanced and the degree of unbalance gradually increases, the stability of the system does not change in principle, so the RPC access structure can take into account the advantages of dynamic control of both arms and high system stability. Under the RPC access structure, the dual arms of the RPC and the ESS work together to achieve efficient utilization of the locomotive regenerative braking energy, while the PV access reduces the long-term operating costs of the rail operator. Due to the better stability of the RPC access structure, the stabilized traction power system reduces the safety risk due to power failures, while allowing for denser train scheduling and increased line capacity.

To verify the conclusions of the stability analysis, a model of the two access structures was built in MATLAB/Simulink. Taking the traction condition as an example, the simulation results are shown in Figs. 15, 16 and 17.

By comparing the DC bus voltage of the two access structures, it can be seen that the DC bus voltage can be stably maintained at 700 V under both structures. The DC bus voltage ripple under the RPC access structure is smaller than that under the VSC access structure, and the AC side output current under the RPC access structure is more stable than that under the VSC access structure. The results under braking condition is similar and will not be discussed here.

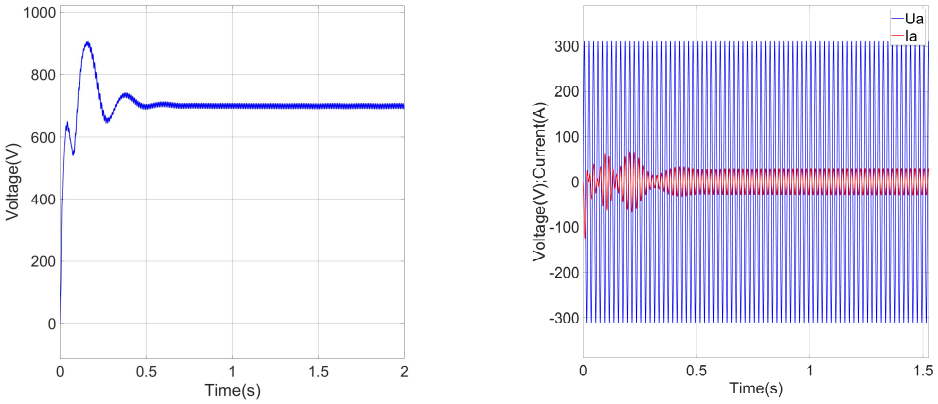

(a) The DC bus voltage (b)

Fig. 15. Simulation waveform under traction condition with RPC access structure

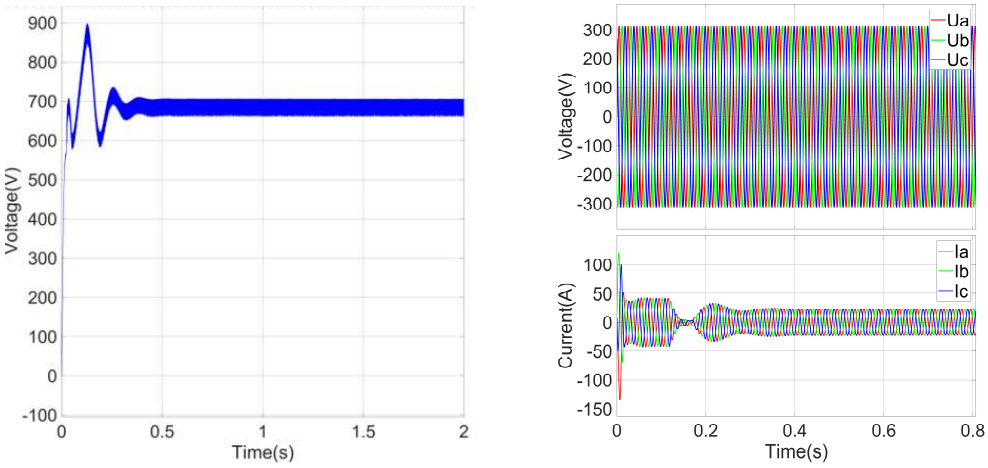

(a) The DC bus voltage (b) The output voltage and output current

Fig. 16. Simulation waveform under traction condition with VSC access structure

The simulation results are consistent with the Nyquist curve results. When a 6.4 kW CPL is connected to the two structures, the DC bus voltage ripple increases in the RPC access structure, and the system stability decreases. In the VSC access structure, the DC bus voltage becomes unstable, and the system is unstable. The results under braking condition is similar and will not be discussed here. Therefore, the simulation results also verify that the RPC access structure of the PV-ESS has higher stability and system robustness than the VSC access structure.

In summary, the system stability analysis, system robustness analysis under the influence of negative impedance characteristics, and system simulation results show that when the same capacity of the PV-ESS is connected to the traction power supply system through the DC bus, when the two structures output the same amount of active power, the RPC access structure has

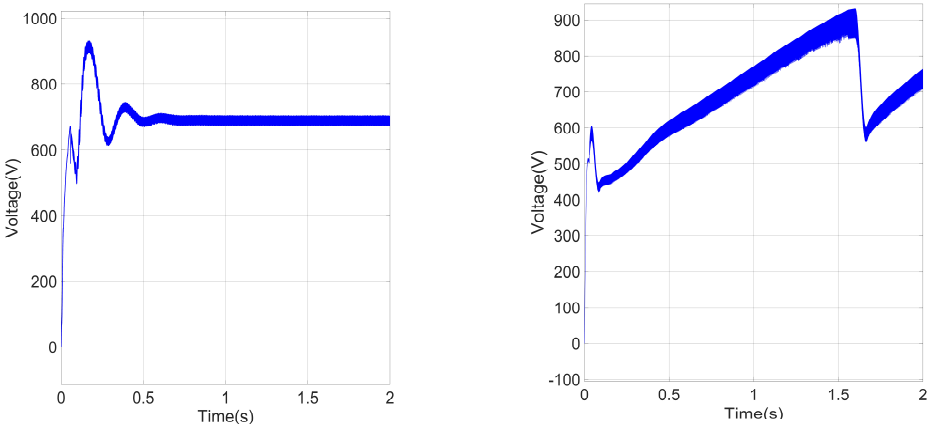

(a) RPC access structure (b) VSC access structure

Fig. 17. Simulation waveform of DC bus voltage after CPL access under traction condition

a greater system stability margin than the VSC access structure, and the RPC access structure has better system robustness. Combined with the RPC access structure, it is also easy to control, prevent power from being returned, and can absorb PV power to the greatest extent. Through comparative analysis of the two, it is more stable and reliable to connect PV and the ESS to the traction power supply system through the RPC access structure.

6. Summary and conclusion

The study begins by developing impedance models for various components of a traction power supply system incorporating PV and the ESS. It then examines two distinct PV-ESS access structures: one utilizing the RPC and another using the VSC. The research analyzes the port impedance characteristics of both the RPC and VSC, considering the effects of system parameter variations and controller parameter adjustments. Subsequently, the paper presents equivalent circuit models for the RPC and VSC under two typical operating conditions. The investigation concludes with an impedance-based stability and adaptability analysis of the traction power supply system for both PV-ESS access structures. Based on this analysis, the following observations are made:

1. The influence of the change in the DC-side capacitance on the input impedance of the two access structures was analyzed. It can be seen from the Bode plot that the change in the DC-side capacitance only affects the resonant peak of the RPC and VSC input impedance, and does not affect the magnitude of the input impedance. If the output filter inductance is not selected properly, the input impedance of the two structures will be inverted, which will affect the stability of the system.
2. Under the RPC access structure, increasing the voltage loop scaling factor will reduce the magnitude of the input impedance. Increasing the voltage loop integration factor will not only affect the resonant frequency of the input impedance, but also increase the magnitude of the input impedance. The situation is similar for the VSC access structure, but when the voltage loop integration factor increases, the magnitude of the input impedance will

decrease. Under both access structures, the current loop factor has little effect on the input impedance. From the impedance ratio Nyquist curve, it can be seen that under traction and braking conditions, an increase in the capacitance on the DC side will improve the stability of the traction power supply system with PV and the ESS under both access structures.

3. This paper starts from the perspective of stability, and under two typical operating conditions, the PV-ESS access capacity under the two access structures is the same, the output and input power of the two arms of the RPC access structure and the VSC access structure are the same, and the control strategies of the two access structures are the same. Compared with the impedance ratio Nyquist curve, the RPC access structure is further away from the forbidden region, so the RPC access structure has higher system stability than the VSC access structure. When the same capacity CPL with negative damping is connected, under the two typical operating conditions, the VSC access structure is more likely to become unstable than the RPC access structure, so the RPC access structure has better system robustness than the VSC access structure. Finally, combined with simulation analysis, it is comprehensively determined that the stability of the traction power supply system with PV and the ESS under the RPC access structure is higher, and it is more suitable as the PV-ESS access structure in the background of a traction power supply system with a high proportion of new energy access.

References

[1] Xianfeng D., Minwu C., Junhong L., Yingtao C., Tianshu C., Ning Z., *Negative Sequence Compensation Method for High-Speed Railway with Integrated Photovoltaic Generation System*, CPSS Transactions on Power Electronics and Applications, vol. 7, no. 2, pp. 130–138 (2022), DOI: 10.24295/CPSST-PEA.2022.00012.

[2] Yinbo G., Haitao H., Junyu C., Ke W., Zhengyou H., *Combined Active and Reactive Power Flow Control Strategy for Flexible Railway Traction Substation Integrated with ESS and PV*, IEEE Transactions on Sustainable Energy, vol. 13, no. 4, pp. 1969–1981 (2022), DOI: 10.1109/TSTE.2022.3178095.

[3] Jianwei Y., Suhua F., Huibin G., Kai L., Yueping X., *Optimal Configuration of Photovoltaic Energy Storage Capacity in Multi-substation Interconnected Traction Power Supply System*, Journal of Southwest Jiaotong University, to be published.

[4] Haitao H., Zheng Z., Zhengyou H., Bo W., Ke W., Xiaowei Y., Wenjing W., *The Framework and Key Technologies of Traffic Energy Internet*, Proceedings of the CSEE, vol. 38, no. 1, pp. 12–24+339 (2018), DOI: 10.13334/j.0258-8013.pcsee.171969.

[5] Wenli D., Chaohua D., Weirong C., *Application of PV Generation in AC/DC Traction Power Supply System and the Key Problem Analysis under the Background of Rail Transit Energy Internet*, Proceedings of the CSEE, vol. 39, no. 19, pp. 5692–5702+5897 (2019), DOI: 10.13334/j.0258-8013.pcsee.181848.

[6] Mingliang W., Chaohua D., Wenli D., Yan G., Huabo C., Weirong C., *Back-to-Back PV Generation System and Its Control Strategy for Electrified Railway*, Power System Technology, vol. 42, no. 2, pp. 541–547 (2018), DOI: 10.13335/j.1000-3673.pst.2017.1709.

[7] Wenli D., Chaohua D., Ai G., Fangli S., Chunbixue H., Mingliang W., *Harmonic interaction influence of PV generation system accessing to traction power supply system and its adaptability analysis*, Electric Power Automation Equipment, vol. 39, no. 4, pp. 181–189 (2019), DOI: 10.16081/j.issn.1006-6047.2019.04.027.

[8] Xia Z., Zijun X., Ying W., *Low-frequency Stability Analysis of Photovoltaic Connected Traction Power Supply System Based on Extended Forbidden Region-based Criterion*, High Voltage Engineering, vol. 49, no. 5, pp. 1997–2007 (2023), DOI: 10.13336/j.1003-6520.hve.20220690.

[9] Cheng J., Xiaojun W., Yao C., Chengjie B., *Research on Stability of Electrified Railway Train-Network Coupling System Based on Improved Forbidden Region Criterion*, Transactions of China Electrotechnical Society, vol. 36, no. 21, pp. 4459–4469 (2021), DOI: 10.19595/j.cnki.1000-6753.tces.L90252.

[10] Xiuqing M., Ying W., Sitong C., Yingchen W., Zhengyou H., *Stability Research on High-Speed Railway Vehicle Network Electric Coupling System Based on Improved Sum-Norm Criterion*, Transactions of China Electrotechnical Society, vol. 34, no. 15, pp. 3253–3264 (2019), DOI: 10.19595/j.cnki.1000-6753.tces.L80594.

[11] Pengkun L., Yue W., Yi L., Quanle Z., Yinglin X., Xuan L., Bole F., Runtian L., *Impedance Modeling and Mechanism Analysis of Low-Frequency Oscillations in Single-Phase MMC-RPC Integrated Vehicle-Grid Coupling System*, IEEE Transactions on Power Electronics, vol. 38, no. 4, pp. 4820–4839 (2023), DOI: 10.1109/TPEL.2022.3233350.

[12] Qian M., Xinpeng M., Pei L., Rijie L., Hao C., *Research on Coordinated Control Strategy of Energy Storage Type Railway Power Conditioner*, IEEE Transactions on Transportation Electrification, vol. 9, no. 1, pp. 182–195 (2023), DOI: 10.1109/TTE.2022.3172166.

[13] Jiayi L., *Design and Verification of Back-to-back Converter for PV/ES Connected to Electrified Railway Traction Power Supply System*, M.D. Thesis, School of Electrical Engineering, Southwest Jiaotong University, Chengdu (2021).

[14] Peng C., Huiwen K., Chao W., Jing M., *Integrated Configuration and Control Strategy for PV Generation in Railway Traction Power Supply Systems*, CSEE Journal of Power and Energy Systems, vol. 8, no. 6, pp. 1603–1612 (2022), DOI: 10.17775/CSEEJPES.2020.03480.

[15] Mingyuan C., Xiaoru W., Xiaoqin L., Rui K., *Modeling and Low-Frequency Oscillation Analysis of an Asymmetrical Traction Power System Connected to Power Grid*, IEEE Transactions on Transportation Electrification, vol. 9, no. 1, pp. 1750–1764 (2023), DOI: 10.1109/TTE.2022.3200994.

[16] Wenli D., Chaohui D., Weirong C., Shibin G., *Experimental Investigation and Adaptability Analysis of Hybrid Traction Power Supply System Integrated with Photovoltaic Sources in AC-Fed Railways*, IEEE Transactions on Transportation Electrification, vol. 7, no. 3, pp. 1750–1764 (2021), DOI: 10.1109/TTE.2021.3053053.

[17] Shaofeng X., Manqi F., Guohua X., *Influence of PV generation system accessing to traction power supply system on power quality*, Electric Power Automation Equipment, vol. 38, no. 10, pp. 53–59 (2018), DOI: 10.16081/j.issn.1006-6047.2018.10.009.

[18] Hanlin W., Xiaohong H., Haoyang L., You P., Tao R., Qunzhan L., *Voltage Coordination Control Method of Three-phase Traction Power Supply System with Distributed Photovoltaic Integration*, High Voltage Engineering, vol. 50, no. 4, pp. 1645–1654 (2024), DOI: 10.13336/j.1003-6520.hve.20221667.

[19] Xue Z., Yi P., Wei D., Ting Y., Shixiong F., Renle H., *Stability Analysis of AC/DC Hybrid Distribution System with Constant Power Loads*, Proceedings of the CSEE, vol. 37, no. 19, pp. 5572–5582+5834 (2017), DOI: 10.13334/j.0258-8013.pcsee.161579.

[20] Mingliang W., *Research on photovoltaic generation technology and its economic performance in electrified railway*, M.D. Thesis, School of Electrical Engineering, Southwest Jiaotong University, Chengdu (2018).

[21] Middlebrook R.D., Cuk S., *A general unified approach to modelling switching-converter power stages*, 1976 IEEE Power Electronics Specialists Conference, Cleveland, USA, pp. 18–34 (1976), DOI: 10.1109/PESC.1976.7072895.

[22] Cad. M. Wildrick *et al.*, *A method of defining the load impedance specification for a stable distributed power system*, IEEE Transactions on Power Electronics, vol. 10, no. 3, pp. 280–285 (1995), DOI: 10.1109/63.387992.

[23] Wenli D., *Research on adaptability and countermeasures of photovoltaic generation system accessing to electrified railway traction power supply system*, M.D. Thesis, School of Electrical Engineering, Southwest Jiaotong University, Chengdu (2019).

[24] Chuanping W., An L., Xianyong X., Fujun M., Juan S., *Integrative Compensation Method of Negative Phase Sequence and Harmonic for High-speed Railway Traction Supply System with V/v Transformer*, Proceedings of the CSEE, vol. 30, no. 16, pp. 111–117 (2010.

[25] Wenjing W., Haitao H., Ke W., Junyu C., Zhengyou H., *Energy Storage Scheme and Control Strategies of High-Speed Railway Based on Railway Power Conditioner*, Transactions of China Electrotechnical Society, vol. 34, no. 6, pp. 1290–1299 (2019), DOI: 10.19595/j.cnki.1000-6753.tces.180287.

[26] Mosaddique Nawaz H., Rahul M., Vivek A., *A Frequency-Dependent Virtual Impedance for Voltage-Regulating Converters Feeding Constant Power Loads in a DC Microgrid*, IEEE Transactions on Industry Applications, vol. 54, no. 6, pp. 5630–5639 (2018), DOI: 10.1109/TIA.2018.2846637.